

SpatialMem: Unified 3D Memory with Metric Anchoring and Fast Retrieval

Xinyi Zheng^{1*}, Yunze Liu², Chi-Hao Wu¹, Fan Zhang¹, Hao Zheng¹, Wenqi Zhou¹,
Walterio W. Mayol-Cuevas¹, Junxiao Shen^{1,2†}

{wf24018, fan.zhang, me24271, bt24001, walterio.mayol-cuevas, junxiao.shen}@bristol.ac.uk,

{yunze.liu, chi-hao.wu, junxiao.shen}@memories.ai,

¹**University of Bristol** ²**Memories.ai Research**

*Equal contribution.

†Corresponding Author

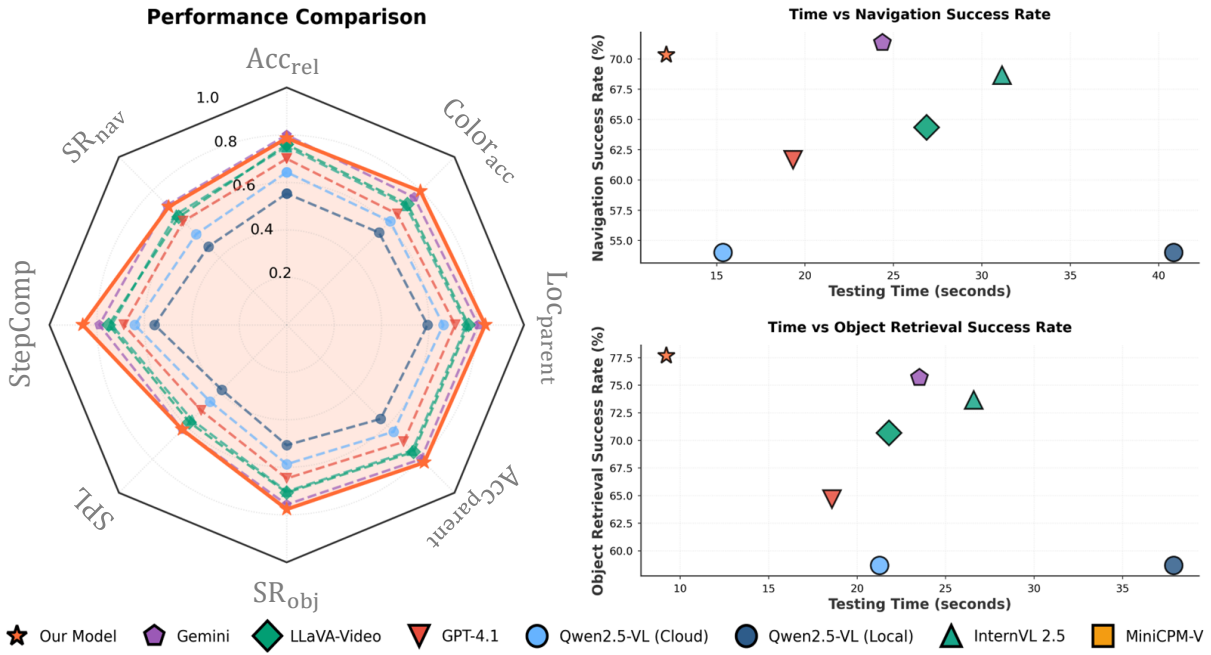


Figure 1. Performance and efficiency comparison of SpatialMem with multimodal baselines. Left: radar plot summarizing accuracy across relative-position reasoning and navigation, averaged over three scenes. Right: testing time vs success rate for navigation (top) and object retrieval (bottom), highlighting task latency and its trade-off with accuracy.

Abstract

We present SpatialMem, a memory-centric system that unifies 3D geometry, semantics, and language into a single, queryable representation. Starting from casually captured egocentric RGB video, SpatialMem reconstructs metrically scaled indoor environments, detects structural 3D anchors (walls, doors, windows) as the first-layer scaffold, and populates a hierarchical memory with open-vocabulary object nodes—linking evidence patches, visual embeddings, and two-layer textual descriptions to 3D coordinates—for compact storage and fast retrieval. This design enables in-

terpretable reasoning over spatial relations (e.g., distance, direction, visibility) and supports downstream tasks such as language-guided navigation and object retrieval without specialized sensors. Experiments across three real-life indoor scenes demonstrate that SpatialMem maintains strong anchor-description-level navigation completion and hierarchical retrieval accuracy under increasing clutter and occlusion, offering an efficient and extensible framework for embodied spatial intelligence.

1. Introduction

Enabling autonomous agents, such as augmented reality (AR) assistants or mobile robots, to robustly understand and

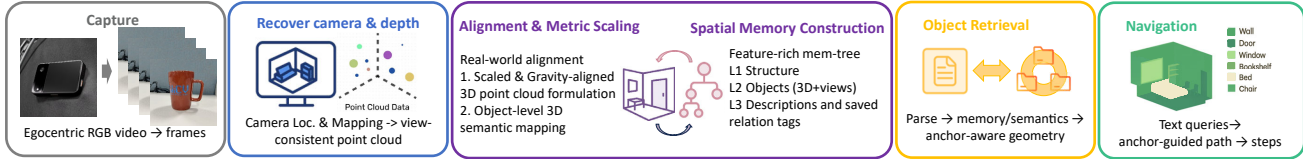


Figure 2. Overview of our pipeline. Our pipeline has five steps: image ingestion normalizes egocentric RGB while preserving parallax and temporal cues; geometry estimation recovers intrinsics/extrinsics and dense depth (e.g., transformer-based) with light bundle adjustment; metric alignment detects the floor, aligns to global z , and sets scale via a height prior; structure and objects are detected, lifted to 3D, and associated to nearby anchors; finally, a rooted memory tree supports path-based relational queries over anchors and object nodes.

interact with 3D indoor environments, requires more than just frame-by-frame perception. A critical component is a persistent, hierarchical spatial memory [1] that grounds language queries in a stable, metric world model. Unlike short-term visual processing, such a memory must maintain consistency over time. This allows for complex relational questions (e.g., “what is on the table to the left of the window?”) by grounding queries in persistent metric anchors like walls, doors, and windows, which, in turn, provide context for dynamic object nodes.

A significant barrier to the deployment of such systems is their reliance on specialized hardware, such as depth sensors (RGB-D) or inertial measurement units (IMUs), and calibrated Visual-SLAM systems [22]. To maximize accessibility and enable low-cost deployment on commodity hardware like mobile phones and egocentric cameras, we target the challenging task of building this 3D queryable memory from casual, egocentric RGB video streams alone.

However, building such a unified memory from monocular 2D images is fraught with challenges. These difficulties are coupled and must be addressed simultaneously. First, accurate camera pose and dense depth must be recovered from monocular streams (Monocular Reconstruction), an inherently ill-posed task that must be robust to motion blur, occlusion, and dynamic lighting conditions. Second, the recovered structure and objects must be aligned to a common metric upright coordinate frame (Metric-Upright Alignment). This alignment ensures that spatial expressions like “next to the door” or “three meters behind the sofa” have precise, actionable geometric meanings. Third, indoor scenes are hierarchical - walls define rooms, which contain objects. Capturing this Hierarchical Context and maintaining it as the environment changes is critical for compositional reasoning and multi-hop retrieval. Finally, the system must support efficient, low-latency updates (Real-time Efficiency), allowing users to query or modify memory in real time, even when dealing with noisy inputs and scene dynamics, making it practical for interactive applications.

To address these challenges, we introduce a hierarchical 3D memory system that unifies geometry, semantics, and language in a single, queryable structure. Our system is

explicitly designed to process RGB-only video inputs and enables complex metric relational queries for spatial reasoning and long-term object retrieval. To support compositional reasoning, we utilize a two-layer description for each object: the first layer captures its general attributes, while the second encodes contextual relations and environment-specific details. By leveraging recent advances in monocular 3D reconstruction [43], open-vocabulary segmentation [41], and language models [36], our system provides interactive querying while grounding all answers in reliable 3D structural anchors with explicit metric relations.

We evaluate SpatialMem on three indoor scenes, demonstrating strong performance in indoor navigation and object retrieval tasks. In Scene 1, our navigation Step Completion is 0.89, slightly ahead of Gemini’s 0.84, with accuracy closely matching at 0.84 compared to Gemini’s 0.85. Despite larger scenes presenting some degradation, our model maintains robust performance. Notably, SpatialMem also demonstrates significantly faster testing times and a smaller model size compared to baselines like Gemini, making it more efficient for real-time applications.

Our main contributions are as follows:

- We introduce a unified, hierarchical 3D memory system built purely from egocentric RGB video, which integrates geometry, semantics, and language into a single queryable structure.
- We propose a novel two-layer object description mechanism that facilitates compositional reasoning by encoding both general attributes and specific contextual relations.
- Our system grounds open-vocabulary language queries in 3D structural anchors (e.g., walls and doors) with explicit metric relations, enabling precise spatial reasoning.
- We demonstrate an efficient architecture that supports low-latency memory updates and real-time querying, proving its practicality for interactive applications on modest hardware.

2. Related Work

3D Reconstruction. Classical pipelines such as COLMAP [29] and ORB-SLAM2 [26] estimate poses and geometry via feature matching and bundle adjustment,

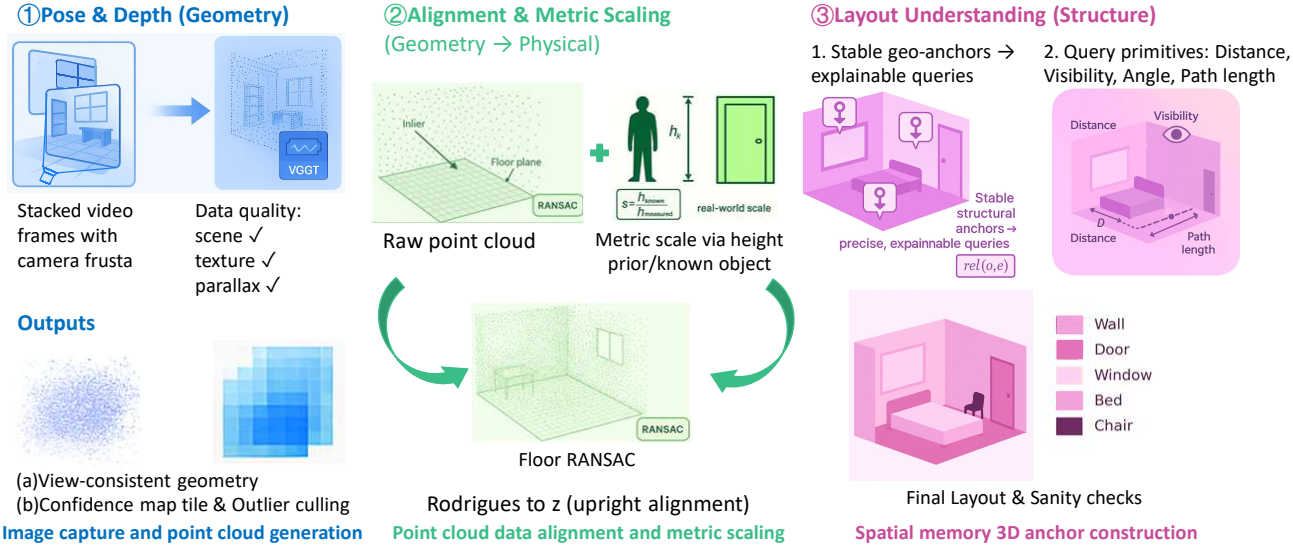


Figure 3. Geometry back-end and metric alignment. We use a feed-forward RGB geometry module and align to an upright, metric frame.

which can present an accurate structure in 3D. However, they are sensitive to calibration in egocentric videos, because those videos usually have more motion blur and it is difficult to obtain a clear bundle adjustment result [23, 24]. To reduce computational cost, newer learning-based methods infer depth and pose directly from RGB, and more recent transformer models (e.g., VGGT [32], SLAM3R [21]) further improve speed and generalization across varied scenes. In our system, these components are swappable back ends: we accept any geometry that is stable enough to host anchors and objects; the novelty lies in the memory we build on top of it.

Scene Layout Understanding. For indoor environments, early layout methods, such as RGB-D room boxes or wall/door/window detectors, provided useful structure but limited relational expression [39, 40, 42]. Afterwards, open-vocabulary integrated vision–language tools, including CLIP [27], GLIP [15], GroundingDINO [20], SAM [12] for masks, captioners for fluent text [5]. These new models greatly broaden category coverage, yet remain 2D and frame-local. Recent scene graphs [33] and LLM-aided parsers [4] move toward structured semantics, but often lack a shared metric frame that fixes direction, distance, and visibility across views [10].

Vision Language Models. Multimodal models connect visual content to language, enabling open-vocabulary recognition and flexible descriptions [18, 35]. From 2D venue, there are already models that would perform well in image–text multi-modal. CLIP established robust image–text embeddings [17]; GLIP and Grounding DINO extend open-vocabulary detection [14, 28]; SAM provides general segmentation [2]; captioning models produce fluent region-

level text [7]. For a longer video, most multimodal methods combine 2D with texts, but they rarely add importance to 3D information. However, most outputs remain 2D and frame-local, lacking a persistent 3D reference that maintains consistency across viewpoints and time [18, 37, 38].

Memory Systems. Early models, such as semantic voxel/TSDF maps [16, 25], fuse recognition into geometry but are computationally heavy because they attempt to recreate every detail at the 3D level [11]. More recent systems move toward open-vocabulary scene graphs [6], multimodal episodic memories (video+text) [9, 31], and vector-database retrieval for scalability [8]. These enable flexible queries but often lack an explicit, shared metric frame, which can easily lead to relative-position errors [13]. These approaches advance semantic breadth and retrieval efficiency, and we build on that progress. The remaining gap is explicit metric grounding: without a common 3D frame, relative position can be inconsistent over time [3, 34]. Our memory targets this gap while preserving open-vocabulary flexibility [19, 30] by anchoring layout, objects, and concise two-layer text (attributes + anchor-relative relations) to the same upright, metric 3D frame, stored in a rooted tree. This yields interpretable nodes/edges, persistent references across views and time, and *relational* queries (distance, direction, visibility) that are fast to update and robust under casual RGB capture.

3. Method

3.1. Problem Setup and Design Principles

We are given a casually captured RGB sequence $\{I_t\}$ with intrinsics K_t and (estimated) extrinsics (R_t, t_t) , from which

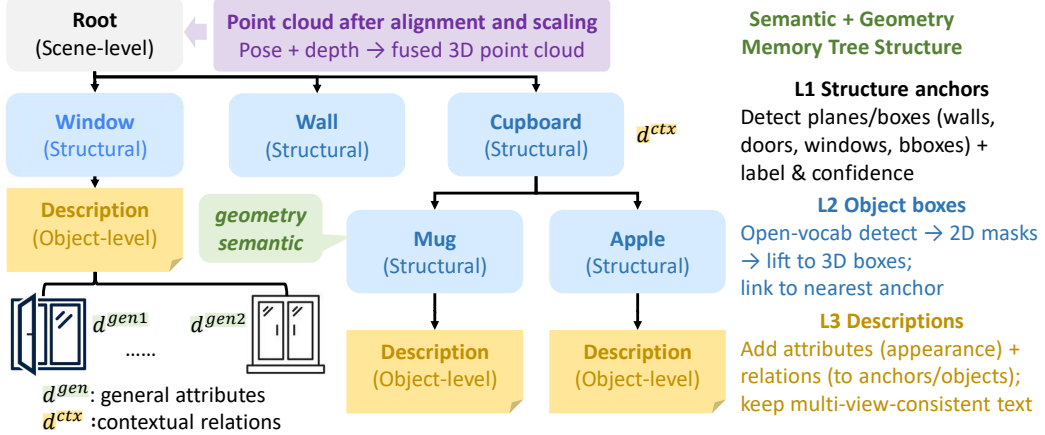


Figure 4. Tree-structured scene memory: anchors (Level-1), objects (Level-2), and two-layer text (Level-3).

we reconstruct a point set P in an upright, metric frame. Our goal is a *unified, metric-anchored scene memory* that supports (i) object/location queries, (ii) relational queries (e.g., “left of the window”), and (iii) navigation/retrieval across time. We store the memory as a rooted tree $T = (V, E)$ with typed nodes/edges defined below.

3.2. 3D Environment Preparation

Our goal is to provide the minimal state that the memory needs: a view-consistent point cloud and camera trajectory in an upright, metric frame, along with a small set of stable structural seeds that initialize Level-1. From egocentric RGB, we estimate camera poses and dense depth with a swappable back-end (e.g., VGGT/SLAM3R/COLMAP), fuse them into a point set P , and align by fitting the floor plane ($\text{normal} \rightarrow +z$), stabilizing the heading, and applying a simple height prior for scale—yielding an allocentric, metric frame with well-defined predicates.

On the aligned geometry, we propose anchors—walls as large vertical planes, and doors/windows as thin vertical openings from edge/depth gaps—then verify across views, merge duplicates, and keep only the consistently supported ones. A proposal is *stable* if it has sufficient point support, multi-view coverage, and temporal persistence. Optionally, we also seed coarse 3D object boxes using an off-the-shelf SpatialLM cue; these remain provisional and are later refined by multi-view evidence within the memory.

Stable anchors are promoted to Level-1 nodes with geometry $G(v)$ (plane/box parameters), semantics $S(v)$ (anchor type), and a confidence score, with links prepared for subsequent object attachment. These seeds initialize the memory tree and anchor the object and description layers introduced next in §3.3.

3.3. Unified Hierarchical Spatial Memory

In this section, we focus on explaining what the main content of the tree structure is and how this information is naturally linked with each other by their 3D positional relations. First, we start with the detailed filling of the tree:

Structure. We maintain $T = (V, E)$ as a rooted, metric hierarchy with four layers:

- **Root:** scene metadata and global frame for certain scene, for indoor scenes will be rooms specifically.
- **Level-1 (Anchors):** structural elements (walls, doors, windows) with oriented planes/boxes initially detected by SpatialLM. This layer will focus more on 3D spaces and generating a preliminary result as a beginning anchor for the following tree building.
- **Level-2 (Objects):** instances linked to 3D boxes and multi-view 2D crops/masks. This layer will focus more on detailed and vision-based content. This vision-based information will be enhanced by a more accurate and centering semantic understanding model, thereby adding more detail based on a 3D framework.
- **Level-3 (Descriptions):** *attributes* (category, color, size, material) and *relations* to anchors/objects. In order to prevent gaining more illusions when adding details to all frames, another layer description is also added in a different layer for overall control which will be shown later. Each node v stores geometry $G(v)$, semantics $S(v)$, and text $D(v)$; edges are parent-child (hierarchy) and typed relations (e.g., near/attached/left-of).

3.4. Metric Grounding and Relational Semantics

After alignment, the world frame is now upright with $+z$ as up, so vertical relations are now uniform and simple for direct saving. We used plain definitions: an object is *on* a support when its bottom is roughly level with the support’s top and their footprints overlap; it is *over/above* when it sits

clearly higher; and *below/under* when it sits clearly lower.

Lateral relations (*left/right/front/behind*) are recorded as frame tags, since viewpoint changes can easily confuse these cues. We reconcile these tags across views using anchors and retain them as view-local hints that can be fused with image understanding at query time, so local queries remain grounded in the intended view and maintain high accuracy. In short, vertical predicates are evaluated once in the global z -aligned frame, while lateral predicates are first egocentric and then consolidated into allocentric relations.

3.5. Two-Layer Descriptions (Attributes \rightarrow Relations)

We describe each scene with two layers. The first layer captures what the current image shows. The second layer keeps a stable summary of the scene that holds across viewpoints. Using both layers makes queries simple: the first layer provides fine, momentary detail, while the second layer provides a reliable reference for downstream tasks.

Layer 1 | Image-level

This layer is tied to the current frame. It records what an object is and where it is relative to nearby 3D anchors and objects, as seen now. We detect and segment objects in 2D, lift them to 3D, and write short phrases that reflect the current view. Because this layer follows the camera, its content may change due to occlusion, lighting, or viewpoint.

Layer 2 | Uniform scene-level

This layer summarizes what remains true across frames. It stores the same kinds of attributes and relations, but only after there is enough agreement from multiple views. Updates are conservative to avoid drift, so the wording remains consistent over time. This layer serves as the default reference for navigation, retrieval, and planning.

All relations in both layers refer to named 3D anchors or objects in the shared metric frame rather than free text. This keeps references stable and makes relational queries resolve to clear paths in the memory graph.

3.6. Query and Retrieval (Low Latency)

We answer queries by walking along the memory graph T . A “locate” query finds the node or nodes whose names and simple geometry match the request (for example, “mug on the desk near the left wall”). A “relational” query follows a short chain of steps in the graph, such as $wall \rightarrow window \rightarrow mug$, while checking distances and directions at each step. Navigation and retrieval transform a natural-language instruction into a sequence of anchor and object waypoints that the system can follow.

To keep this fast, nodes are organized by type and by 3D region, so a query only looks at nearby candidates. The checks are lightweight—mainly distance, relative orientation (left/right/front/back), and visibility tests. The MEM-

Table 1. RGB-only ingestion and inference settings (Lucia device).

Vision (RGB only)	
Native image resolution (egocentric)	3840×2160 (photo), 2016×1512 @30fps
Normalized ingestion resolution	1024×768–1920×1080
Inference resolution (geometry back-end)	640×480–1024×768
Frame sampling interval	1–2 s (0.5–1 Hz)

ORYUPDATE procedure maintains these indexes as new frames arrive, so the response time remains short. Full algorithms and caching details are provided in the Appendix.

3.7. Training and Implementation Notes

We keep the main text model-agnostic and concise; schedules, thresholds, and ablation scaffolding move to the Appendix. The online variant streams frames from a wearable/phone; this is an engineering path that does not alter the representation. Table 1 summarizes high-level I/O and interaction latencies (moved from ingestion for clarity).

4. Experimental Setup

We evaluate three egocentric, real-life indoor scenes captured by ourselves using a lightweight pin camera (LUCI). For each scene, we reconstruct a metric 3D memory from RGB images; capture and pre-processing follow the Method section.

- **Scene 1 (Simple room):** A simple and compact indoor space with only major furniture and a few small objects (e.g., a cushion, a mug).
- **Scene 2 (Suite main room):** A more complicated room with multiple major pieces of furniture and objects inside compared to Scene 1.
- **Scene 3 (Laboratory/storage):** A very challenging environment of a real engineering laboratory, with many heterogeneous items.

These scenes span low→high complexity and are used consistently across all tasks.

4.1. Metrics

We arranged our metrics based on the features of the tasks that we specifically tried. After separating the experiments into three types — Basic (relative position), Application: navigation, and Application: object retrieval — we built our evaluation system in the following sections.

Notation. Let \mathcal{D} be the set of episodes. For episode $i \in \mathcal{D}$, denote goal g_i , final user location \hat{g}_i , shortest path L_i^* , executed path L_i , and use the indicator $\mathbf{1}[\cdot]$. Navigation uses a distance d_{thr} , proximity thresholds $\tau_{\text{near}}, \tau_{\text{attach}}$, and angular tolerance θ_{rel} .

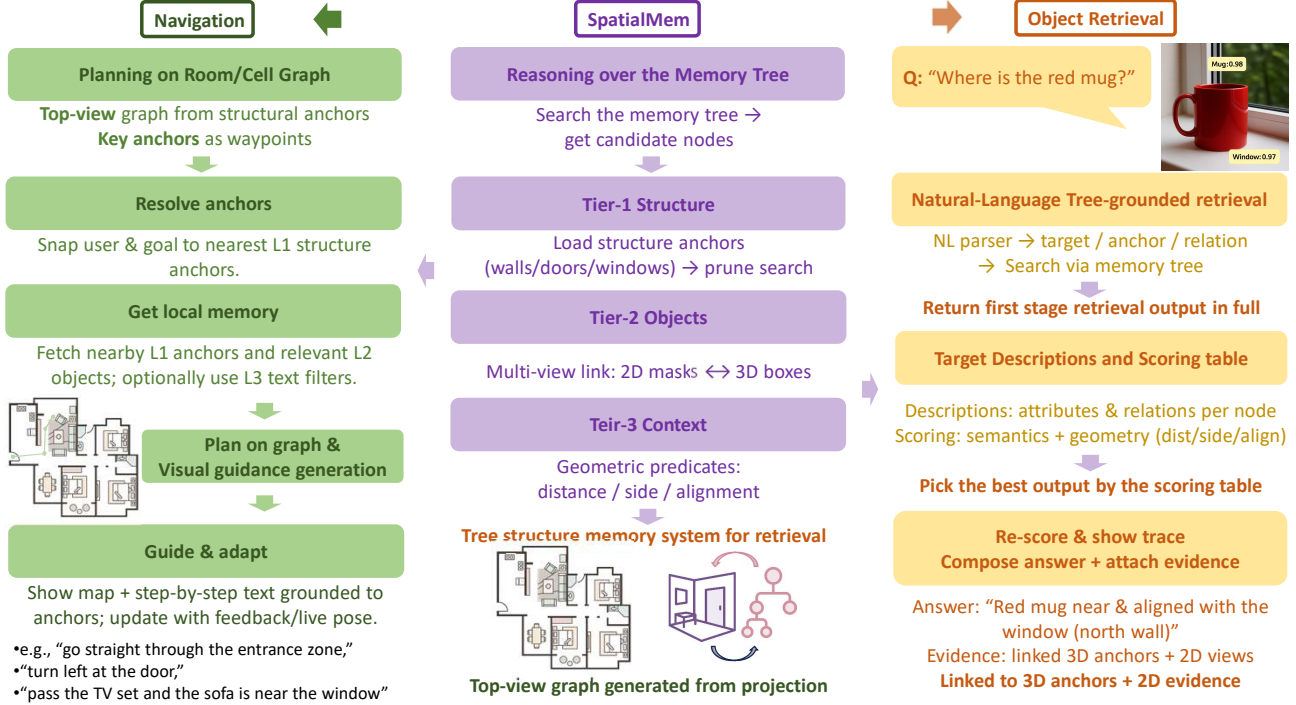


Figure 5. Overview of SpatialMem pipeline. The memory tree (center) organizes structural anchors, objects, and contextual relations. Left: navigation uses the anchor graph to resolve user/goal locations and generate step-by-step graph guidance. Right: object retrieval parses a language query, searches the tree, and returns an answer with linked 3D anchors and 2D evidence.

Task 1 | Basic (relative position)

This task assesses whether memory recovers basic spatial relations between entities (left, right, front, behind, near, on). Each query specifies two targets, and the system returns a natural-language answer in the form “A is *rel* of B.”

Accuracy. The primary metric is *Relation Accuracy* (Acc_{rel}): the fraction of queries whose predicted relation matches the 3D annotation. To diagnose stability around structures, we report *Anchor-Specific Relation Accuracy* ($Acc_{rel}(s)$): the same accuracy computed per anchor type or level (e.g., walls, doors, windows), then macro-averaged.

Evaluation frame. Relations such as left/right/front/behind are evaluated in an allocentric frame with a fixed angular tolerance; near/attached use distance thresholds to the plane or box anchor. We macro-average over anchors and include a light audit for ambiguous boundary cases.

Task 2 | Application: navigation

We report four metrics: *success*, *step completion*, *efficiency*, and *error*.

Success rate (SR_{nav}). An episode is successful if the final predicted goal lies within a threshold d_{thr} of the true target; SR_{nav} is the fraction of successful episodes.

Step completion ($StepComp$). For episodes with sub-steps, we compute a weighted completion score per episode

and then average:

$$StepComp_i = \frac{\sum_t w_{i,t} c_{i,t}}{\sum_t w_{i,t}}, \quad (1)$$

$$\overline{StepComp} = \frac{1}{|\mathcal{D}|} \sum_i StepComp_i, \quad (2)$$

$c_{i,t} \in \{0, 1\}$ indicates step success and $w_{i,t}$ is its weight.

Efficiency (SPL). We use the standard Success-weighted by Path Length:

$$SPL = \frac{1}{|\mathcal{D}|} \sum_i S_i^{nav} \cdot \frac{L_i^*}{\max(L_i, L_i^*)},$$

where $S_i^{nav} = 1$ for successful episodes and 0 otherwise, L_i^* is the shortest-path length to the goal, and L_i is the executed path length.

Navigation error (NE). Mean final distance to the goal, computed over failed episodes only. Distance thresholds, angular tolerances, and tie-breaking rules are specified in the Appendix.

Task 3 | Application: object retrieval

We measure retrieval success and hierarchical correctness. This section is focused on evaluating

Retrieval success. Retrieval success SR_{obj} is the proportion of episodes in which the target object is correctly confirmed (set $R_i=1$ if confirmed, otherwise 0); when retrieval depends on navigation, an episode counts as successful only if both the goal is reached and the object is confirmed, and we also report the two components separately.

Hierarchical correctness. Hierarchical correctness evaluates object placement in the memory tree: Acc_{parent} is the share of episodes where the predicted parent node matches the ground truth, while Acc_{path} is stricter—the root→leaf path must match. Both are reported as proportions.

Description quality. $Color\ Acc$ (attribute verification), $Loc@parent$ and $Loc@path$ (location phrase matches parent container or the full root→leaf path).

Metrics summary. We provide per-scene metrics, success tables include Acc_{rel} (overall and per Level-1 anchor), SR_{nav} , $StepComp$, SPL , NE , SR_{obj} , Acc_{parent} , and Acc_{path} .

4.2. Instruction Quality & Error Analysis

We summarize errors as simple proportions. For each category below, we report its share of all errors in the evaluation and a brief subtype breakdown.

Perception/Memory error (Task 1 — Basic). Share of all errors due to sensing or memory (hallucination, wrong recognition, mislocalization). We also report the fraction of each subtype within this category.

Planning error (Task 2 — Navigation). Share of all errors caused by planning (failed to reach goal, missed/incorrect steps, wrong order, inefficient detours). We report both (i) each subtype’s share within planning and (ii) each subtype’s global share among all errors.

Reasoning error (Task 3 — Retrieval). Share of all errors attributed to reasoning (critical mistakes, insufficient exploration, spatial reasoning errors). We also give subtype fractions within this category.

Labeling protocol. Two raters annotated execution traces (video, poses, memory snapshots) with adjudication; agreement scores and visualizations are in the supplement.

5. Results

In this section, we built different basic tasks to evaluate the overall understanding of this memory system and see whether it can support real-life scenarios.

5.1. Layout Understanding

In the basic relative-direction tasks, as shown in the table column **’Basic: Relative Position’**, with a total of 1,500 experiments across three scenes, our model is consistently competitive with the strongest baselines. The overall accuracy of SpatialMem in those tasks is around 0.84/0.78/0.74 for Scenes 1-3, closely tracking the Gemini model, which has an accuracy of around 0.86/0.80/0.74. Overall, the strongest performance appears to be thin layer object, the

window, which is 0.88 detected by SpatialMem but slightly weaker in $Acc_{rel}(\text{Wall})$ compared to Gemini. For those important anchors that shapes the indoor environment and object ranges, our model achieves roughly the same level as Gemini model and has a steady reproducibility.

Seeing the data across three scenes, considering the complexity of the second and third scenes, the degradation of the result seems reasonable. At the same time, even when compared with these three scenes, our model maintains its stable performance, which demonstrates robustness across varying scene complexities. For scene 3, the Qwen and MiniCPM models show a significant performance drop, indicating poor generalization. In short, our model shows its overall excellent and robust performance with an extra short execution time, as shown in Fig 2.

5.2. Indoor Navigation

For the navigation task, our model, designed for memory storage and retrieval, does not focus on detailed coordinate-level path planning like SLAM systems. Instead, it locates the target object and generates step-by-step path planning suitable for human interaction or real-time queries.

In Scene 1, our model achieves the highest Step Completion (0.89), outperforming Gemini (0.84), demonstrating strong navigation consistency. Path Efficiency is also competitive, with our Success-Weighted Path Length (SPL) of 0.67, close to Gemini’s 0.68. However, our model has a lower Success Rate (SR_{nav} : 65) and a higher Final Error (NE : 3.9 m) compared to the baseline, though these differences do not notably impact overall performance.

Across scenes, scene complexity impacts results; yet, most models maintain strong Step Completion and Path Efficiency. Our model shows consistent Step Completion (0.86 in Scene 2, 0.83 in Scene 3) and effectively encodes structural cues for navigation. In more complex scenes (e.g., laboratory storage), challenges such as clutter and occlusion increase Final Error (NE : 4.3 m in Scene 2, NE : 4.8 m in Scene 3). Despite this, the model’s performance remains acceptable for image-based input and practical navigation tasks.

5.3. Object Retrieval Task Analysis

In Scene 1, the model excels in object retrieval with a success rate (SR_{obj}) of 0.72, demonstrating strong hierarchical accuracy ($Acc_{parent} = 0.73$, $Acc_{path} = 0.66$) and solid description-based localization ($Loc@parent = 0.82$, $Loc@path = 0.68$), closely matching the top baseline, Together (0.84/0.73). Color accuracy (0.71) is slightly lower than the baseline (0.80), but this difference is minor.

As the complexity of the environment increases in Scenes 2 and 3, performance declines. In Scene 2, SR_{obj} drops to 0.69, and in Scene 3 to 0.65. Hierarchical accuracy also decreases, but the model remains competitive against

Table 2. Scene 1 — Simple room: overall results across tasks. Higher is better (\uparrow) except NE (\downarrow). Metrics follow Sec. 4.1.

Model	Basic: Relative Position				SR _{nav} \uparrow	Application: Navigation			Application: Object Retrieval			Description Quality		
	Acc _{rel} \uparrow	Acc _{rel} (Wall) \uparrow	Acc _{rel} (Door) \uparrow	Acc _{rel} (Window) \uparrow		StepComp \uparrow	SPL \uparrow	NE [m] \downarrow	SR _{obj} \uparrow	Acc _{parent} \uparrow	Acc _{path} \uparrow	Color Acc \uparrow	Loc@parent \uparrow	Loc@path \uparrow
gemini (Google Gemini)	0.86	0.90	0.82	0.83	0.78	0.84	0.68	3.2	0.81	0.85	0.74	0.80	0.84	0.73
internvl (InternVL 2.5, Local)	0.84	0.88	0.80	0.81	0.75	0.82	0.65	3.4	0.79	0.83	0.71	0.78	0.82	0.71
llava (LLaVA-Video, Local)	0.82	0.86	0.78	0.79	0.72	0.80	0.63	3.6	0.76	0.81	0.69	0.76	0.80	0.69
internvl (InternVL 2.5, Local)	0.78	0.83	0.74	0.75	0.66	0.75	0.58	3.9	0.72	0.77	0.64	0.72	0.77	0.64
openai (OpenAI GPT-4o)	0.76	0.81	0.72	0.73	0.64	0.73	0.56	4.1	0.70	0.75	0.62	0.70	0.75	0.62
together (Qwen2.5-VL, Cloud)	0.70	0.77	0.66	0.67	0.58	0.68	0.50	4.6	0.64	0.69	0.56	0.66	0.70	0.58
qwen2svl (Qwen2.5-VL, Local)	0.60	0.68	0.55	0.56	0.48	0.59	0.42	5.3	0.55	0.60	0.47	0.58	0.62	0.50
Our Model	0.84	0.88	0.82	0.82	0.77	0.89	0.69	3.1	0.83	0.86	0.76	0.82	0.86	0.72
Counts (episodes)	N _{rel} = 500				N _{nav} = 500				N _{obj} = 500				N _{obj} = 500	

Table 3. Scene 2 — Suite main room: overall results across tasks. Higher is better (\uparrow) except NE (\downarrow).

Model	Basic: Relative Position				SR _{nav} \uparrow	Application: Navigation			Application: Object Retrieval			Description Quality		
	Acc _{rel} \uparrow	Acc _{rel} (Wall) \uparrow	Acc _{rel} (Door) \uparrow	Acc _{rel} (Window) \uparrow		StepComp \uparrow	SPL \uparrow	NE [m] \downarrow	SR _{obj} \uparrow	Acc _{parent} \uparrow	Acc _{path} \uparrow	Color Acc \uparrow	Loc@parent \uparrow	Loc@path \uparrow
gemini (Google Gemini)	0.80	0.85	0.76	0.77	0.78	0.79	0.62	3.6	0.76	0.80	0.69	0.76	0.81	0.69
internvl (InternVL 2.5, Local)	0.78	0.83	0.74	0.75	0.79	0.77	0.60	3.8	0.74	0.78	0.67	0.74	0.79	0.67
llava (LLaVA-Video, Local)	0.76	0.81	0.72	0.73	0.72	0.75	0.58	4.0	0.71	0.76	0.64	0.72	0.77	0.64
internvl (InternVL 2.5, Local)	0.72	0.78	0.68	0.69	0.70	0.71	0.53	4.3	0.67	0.72	0.60	0.68	0.73	0.60
openai (OpenAI GPT-4o)	0.70	0.76	0.66	0.67	0.72	0.69	0.51	4.5	0.65	0.70	0.58	0.66	0.71	0.58
together (Qwen2.5-VL, Cloud)	0.65	0.72	0.61	0.62	0.65	0.64	0.46	5.0	0.59	0.64	0.52	0.62	0.66	0.54
qwen2svl (Qwen2.5-VL, Local)	0.56	0.64	0.51	0.52	0.54	0.55	0.39	5.7	0.51	0.56	0.44	0.55	0.59	0.47
Our Model	0.78	0.84	0.75	0.75	0.80	0.86	0.62	3.7	0.78	0.82	0.71	0.79	0.83	0.66
Counts (episodes)	N _{rel} = 500				N _{nav} = 500				N _{obj} = 500				N _{obj} = 500	

Degradation vs. Scene 1 reflects increased clutter/occlusion and longer paths.

Table 4. Scene 3 — Laboratory / storage: overall results across tasks. Higher is better (\uparrow) except NE (\downarrow).

Model	Basic: Relative Position				SR _{nav} \uparrow	Application: Navigation			Application: Object Retrieval			Description Quality		
	Acc _{rel} \uparrow	Acc _{rel} (Wall) \uparrow	Acc _{rel} (Door) \uparrow	Acc _{rel} (Window) \uparrow		StepComp \uparrow	SPL \uparrow	NE [m] \downarrow	SR _{obj} \uparrow	Acc _{parent} \uparrow	Acc _{path} \uparrow	Color Acc \uparrow	Loc@parent \uparrow	Loc@path \uparrow
gemini (Google Gemini)	0.74	0.80	0.70	0.71	0.58	0.74	0.57	4.0	0.70	0.75	0.64	0.72	0.77	0.63
internvl (InternVL 2.5, Local)	0.72	0.78	0.68	0.69	0.52	0.72	0.55	4.2	0.68	0.73	0.62	0.70	0.75	0.61
llava (LLaVA-Video, Local)	0.70	0.76	0.66	0.67	0.49	0.70	0.53	4.4	0.65	0.70	0.59	0.68	0.73	0.59
internvl (InternVL 2.5, Local)	0.66	0.72	0.62	0.63	0.53	0.66	0.48	4.8	0.61	0.66	0.55	0.64	0.69	0.55
openai (OpenAI GPT-4o)	0.64	0.70	0.60	0.61	0.49	0.64	0.46	5.0	0.59	0.64	0.53	0.62	0.67	0.53
together (Qwen2.5-VL, Cloud)	0.58	0.66	0.54	0.55	0.39	0.60	0.41	5.5	0.53	0.58	0.47	0.57	0.62	0.49
qwen2svl (Qwen2.5-VL, Local)	0.50	0.59	0.46	0.47	0.38	0.53	0.35	6.1	0.46	0.52	0.41	0.52	0.57	0.44
Our Model	0.74	0.81	0.62	0.72	0.54	0.83	0.58	4.6	0.72	0.78	0.62	0.78	0.77	0.69
Counts (episodes)	N _{rel} = 500				N _{nav} = 500				N _{obj} = 500				N _{obj} = 500	

the strongest cloud baseline (Together: SR_{obj} = 0.76/0.70, Acc_{path} = 0.69/0.64).

Localization remains strong in cluttered scenes, with Loc@parent and Loc@path in Scene 2 (0.79/0.76) and Scene 3 (0.65/0.61) showing only a small gap compared to the baseline (0.81/0.77 and 0.69/0.63).

The main limitation is in handling fine-grained details, like shelf levels, especially when image cues are sparse. Future improvements should focus on reducing attribute noise and enhancing small-object disambiguation, possibly through multi-view integration.

Overall, the model performs well in object retrieval and localization, with potential for improvement in handling fine-grained details in more cluttered environments.

5.4. Description Quality

In Scene 1, our model achieved a Color Accuracy of 0.71, which is competitive but slightly lower than that of the top baseline model. Together with a Color Accuracy of 0.80. The Localization accuracy was strong, with Loc@parent reaching 0.82, and Loc@path at 0.68, close to the baseline's Loc@parent (0.84) and Loc@path (0.73). As we moved to Scene 2, the model saw a decline, with Color Accuracy

dropping to 0.69, but Localization accuracy (Loc@parent = 0.79, Loc@path = 0.65) remained relatively close to the top baseline. In Scene 3, there was further degradation, particularly in Color Accuracy (0.66), but Localization accuracy was strong (Loc@parent = 0.76, Loc@path = 0.61), with gaps to the best baseline narrowing for path localization. The overall trend suggests that the Localization components remain reliable even in cluttered environments, whereas Color Accuracy faces challenges in more complex scenes due to lighting and small object recognition.

6. Conclusion

We present SpatialMem, a memory-centric system for indoor navigation and object retrieval that unifies geometry, semantics, and language into a single, queryable representation. From egocentric RGB input, our pipeline reconstructs an upright, metric 3D structure, attaches open-vocabulary objects to structural anchors, and assigns concise, two-layer descriptions encoding attributes and anchor-relative relations. Evaluations of core capabilities—layout understanding, instruction-based navigation, and object retrieval—demonstrated high success and efficiency. The results indicate that explicit anchoring and preserved lo-

cal relations yield robust step-wise execution and competitive path efficiency. Future work will focus on broadening usability (e.g., diverse environments, incremental updates, and richer interaction) rather than re-architecting the core. We view SpatialMem as a practical step toward language-driven spatial intelligence for everyday indoor environments.

References

- [1] Valts Blukis, Chris Paxton, Dieter Fox, Animesh Garg, and Yoav Artzi. A persistent spatial semantic representation for high-level natural language instruction execution. In *Conference on Robot Learning*, pages 706–717. PMLR, 2022. [2](#)
- [2] Keyan Chen, Chenyang Liu, Hao Chen, Haotian Zhang, Wenyuan Li, Zhengxia Zou, and Zhenwei Shi. Rsprompter: Learning to prompt for remote sensing instance segmentation based on visual foundation model. *IEEE Transactions on Geoscience and Remote Sensing*, 62:1–17, 2024. [3](#)
- [3] Shizhe Chen, Pierre-Louis Guhur, Makarand Tapaswi, Cordelia Schmid, and Ivan Laptev. Language conditioned spatial relation reasoning for 3d object grounding. *Advances in neural information processing systems*, 35:20522–20535, 2022. [3](#)
- [4] Alberto Coffrini, Mohammad Amin Zadenoori, Paolo Baracochi, Francesco Furfari, Antonino Crivello, and Alessio Ferrari. Toward a method for llm-enabled indoor navigation. *arXiv preprint arXiv:2503.11702*, 2025. [3](#)
- [5] Taraneh Ghandi, Hamidreza Pourreza, and Hamidreza Mahyar. Deep learning approaches on image captioning: A review. *ACM Computing Surveys*, 56(3):1–39, 2023. [3](#)
- [6] Tao He, Lianli Gao, Jingkuan Song, and Yuan-Fang Li. Towards open-vocabulary scene graph generation with prompt-based finetuning. In *European conference on computer vision*, pages 56–73. Springer, 2022. [3](#)
- [7] Simao Herdade, Armin Kappeler, Kofi Boakye, and Joao Soares. Image captioning: Transforming objects into words. *Advances in neural information processing systems*, 32, 2019. [3](#)
- [8] Fan Hu, Aozhu Chen, Ziyue Wang, Fangming Zhou, Jianfeng Dong, and Xirong Li. Lightweight attentional feature fusion: A new baseline for text-to-video retrieval. In *European conference on computer vision*, pages 444–461. Springer, 2022. [3](#)
- [9] Nathan Hughes, Yun Chang, and Luca Carlone. Hydra: A real-time spatial perception system for 3d scene graph construction and optimization. *arXiv preprint arXiv:2201.13360*, 2022. [3](#)
- [10] Nathan Hughes, Yun Chang, and Luca Carlone. Hydra: A real-time spatial perception system for 3d scene graph construction and optimization. *arXiv preprint arXiv:2201.13360*, 2022. [3](#)
- [11] Bernhard Kerbl, Georgios Kopanas, Thomas Leimkühler, and George Drettakis. 3d gaussian splatting for real-time radiance field rendering. *ACM Transactions on Graphics*, 42(4), 2023. [3](#)
- [12] Alexander Kirillov, Eric Mintun, Nikhila Ravi, Hanzi Mao, Chloe Rolland, Laura Gustafson, Tete Xiao, Spencer Whitehead, Alexander C Berg, Wan-Yen Lo, et al. Segment anything. In *Proceedings of the IEEE/CVF international conference on computer vision*, pages 4015–4026, 2023. [3](#)
- [13] Vincent Leroy, Yohann Cabon, and Jérôme Revaud. Grounding image matching in 3d with mast3r. In *European Conference on Computer Vision*, pages 71–91. Springer, 2024. [3](#)
- [14] Liunian Li, Zi-Yi Dou, Nanyun Peng, and Kai-Wei Chang. Desco: Learning object recognition with rich language descriptions. *Advances in Neural Information Processing Systems*, 36:37511–37526, 2023. [3](#)
- [15] Liunian Harold Li, Pengchuan Zhang, Haotian Zhang, Jianwei Yang, Chunyuan Li, Yiwu Zhong, Lijuan Wang, Lu Yuan, Lei Zhang, Jenq-Neng Hwang, et al. Grounded language-image pre-training. In *Proceedings of the IEEE/CVF conference on computer vision and pattern recognition*, pages 10965–10975, 2022. [3](#)
- [16] Yiming Li, Zhiding Yu, Christopher Choy, Chaowei Xiao, Jose M Alvarez, Sanja Fidler, Chen Feng, and Anima Anandkumar. Voxformer: Sparse voxel transformer for camera-based 3d semantic scene completion. In *Proceedings of the IEEE/CVF conference on computer vision and pattern recognition*, pages 9087–9098, 2023. [3](#)
- [17] Feng Liang, Bichen Wu, Xiaoliang Dai, Kunpeng Li, Yinan Zhao, Hang Zhang, Peizhao Zhang, Peter Vajda, and Diana Marculescu. Open-vocabulary semantic segmentation with mask-adapted clip. In *Proceedings of the IEEE/CVF conference on computer vision and pattern recognition*, pages 7061–7070, 2023. [3](#)
- [18] Xiongkun Linghu, Jiangyong Huang, Xuesong Niu, Xiaojian Shawn Ma, Baoxiong Jia, and Siyuan Huang. Multi-modal situated reasoning in 3d scenes. *Advances in Neural Information Processing Systems*, 37:140903–140936, 2024. [3](#)
- [19] Jiazhou Liu, Kadek Ananta Satriadi, Barrett Ens, and Tim Dwyer. Investigating the effects of physical landmarks on spatial memory for information visualisation in augmented reality. In *2024 IEEE International Symposium on Mixed and Augmented Reality (ISMAR)*, pages 289–298. IEEE, 2024. [3](#)
- [20] Shilong Liu, Zhaoyang Zeng, Tianhe Ren, Feng Li, Hao Zhang, Jie Yang, Qing Jiang, Chunyuan Li, Jianwei Yang, Hang Su, et al. Grounding dino: Marrying dino with grounded pre-training for open-set object detection. In *European conference on computer vision*, pages 38–55. Springer, 2024. [3](#)
- [21] Yuzheng Liu, Siyan Dong, Shuzhe Wang, Yingda Yin, Yanchao Yang, Qingnan Fan, and Baoquan Chen. Slam3r: Real-time dense scene reconstruction from monocular rgb videos. In *Proceedings of the Computer Vision and Pattern Recognition Conference*, pages 16651–16662, 2025. [3](#)
- [22] Andréa Macario Barros, Maugan Michel, Yoann Moline, Gwenolé Corre, and Frédéric Carrel. A comprehensive survey of visual slam algorithms. *Robotics*, 11(1):24, 2022. [2](#)
- [23] Armin Masoumian, Hatem A Rashwan, Julián Cristiano, M Salman Asif, and Domenec Puig. Monocular depth estimation using deep learning: A review. *Sensors*, 22(14):5353, 2022. [3](#)

[24] Ben Mildenhall, Pratul P Srinivasan, Matthew Tancik, Jonathan T Barron, Ravi Ramamoorthi, and Ren Ng. Nerf: Representing scenes as neural radiance fields for view synthesis. *Communications of the ACM*, 65(1):99–106, 2021. 3

[25] Alexander Millane, Zachary Taylor, Helen Oleynikova, Juan Nieto, Roland Siegwart, and César Cadena. C-blox: A scalable and consistent tsdf-based dense mapping approach. In *2018 IEEE/RSJ international conference on intelligent robots and systems (IROS)*, pages 995–1002. IEEE, 2018. 3

[26] Raul Mur-Artal and Juan D Tardós. Orb-slam2: An open-source slam system for monocular, stereo, and rgbd cameras. *IEEE transactions on robotics*, 33(5):1255–1262, 2017. 2

[27] Alec Radford, Jong Wook Kim, Chris Hallacy, Aditya Ramesh, Gabriel Goh, Sandhini Agarwal, Girish Sastry, Amanda Askell, Pamela Mishkin, Jack Clark, et al. Learning transferable visual models from natural language supervision. In *International conference on machine learning*, pages 8748–8763. PMLR, 2021. 3

[28] Tianhe Ren, Qing Jiang, Shilong Liu, Zhaoyang Zeng, Wenlong Liu, Han Gao, Hongjie Huang, Zhengyu Ma, Xiaoke Jiang, Yihao Chen, et al. Grounding dino 1.5: Advance the “edge” of open-set object detection. *arXiv preprint arXiv:2405.10300*, 2024. 3

[29] Johannes Lutz Schönberger and Jan-Michael Frahm. Structure-from-motion revisited. In *Conference on Computer Vision and Pattern Recognition (CVPR)*, 2016. 2

[30] Haochen Wang, Cilin Yan, Shuai Wang, Xiaolong Jiang, Xu Tang, Yao Hu, Weidi Xie, and Efstratios Gavves. Towards open-vocabulary video instance segmentation. In *proceedings of the IEEE/CVF international conference on computer vision*, pages 4057–4066, 2023. 3

[31] Junbo Wang, Wei Wang, Yan Huang, Liang Wang, and Tieniu Tan. M3: Multimodal memory modelling for video captioning. In *Proceedings of the IEEE conference on computer vision and pattern recognition*, pages 7512–7520, 2018. 3

[32] Jianyuan Wang, Minghao Chen, Nikita Karaev, Andrea Vedaldi, Christian Rupprecht, and David Novotny. Vggt: Visual geometry grounded transformer. In *Proceedings of the Computer Vision and Pattern Recognition Conference*, pages 5294–5306, 2025. 3

[33] Abdelrhman Werby, Chenguang Huang, Martin Büchner, Abhinav Valada, and Wolfram Burgard. Hierarchical open-vocabulary 3d scene graphs for language-grounded robot navigation. In *First Workshop on Vision-Language Models for Navigation and Manipulation at ICRA 2024*, 2024. 3

[34] Yuyang Yin, Dejia Xu, Zhangyang Wang, Yao Zhao, and Yunchao Wei. 4dgen: Grounded 4d content generation with spatial-temporal consistency. *arXiv preprint arXiv:2312.17225*, 2023. 3

[35] Jingyi Zhang, Jiaxing Huang, Sheng Jin, and Shijian Lu. Vision-language models for vision tasks: A survey. *IEEE transactions on pattern analysis and machine intelligence*, 46(8):5625–5644, 2024. 3

[36] Zeyu Zhang, Quanyu Dai, Xiaohe Bo, Chen Ma, Rui Li, Xu Chen, Jieming Zhu, Zhenhua Dong, and Ji-Rong Wen. A survey on the memory mechanism of large language model-based agents. *ACM Transactions on Information Systems*, 43(6):1–47, 2025. 2

[37] Yaoyao Zhong, Wei Ji, Junbin Xiao, Yicong Li, Weihong Deng, and Tat-Seng Chua. Video question answering: Datasets, algorithms and challenges. In *Proceedings of the 2022 conference on empirical methods in natural language processing*, pages 6439–6455, 2022. 3

[38] Luwei Zhou, Yingbo Zhou, Jason J Corso, Richard Socher, and Caiming Xiong. End-to-end dense video captioning with masked transformer. In *Proceedings of the IEEE conference on computer vision and pattern recognition*, pages 8739–8748, 2018. 3

[39] Wujie Zhou, Enquan Yang, Jingsheng Lei, Jian Wan, and Lu Yu. Pgdenet: Progressive guided fusion and depth enhancement network for rgbd indoor scene parsing. *IEEE Transactions on Multimedia*, 25:3483–3494, 2022. 3

[40] Wujie Zhou, Enquan Yang, Jingsheng Lei, and Lu Yu. Frnet: Feature reconstruction network for rgbd indoor scene parsing. *IEEE Journal of Selected Topics in Signal Processing*, 16(4):677–687, 2022. 3

[41] Chaoyang Zhu and Long Chen. A survey on open-vocabulary detection and segmentation: Past, present, and future. *IEEE Transactions on Pattern Analysis and Machine Intelligence*, 46(12):8954–8975, 2024. 2

[42] Chuhang Zou, Jheng-Wei Su, Chi-Han Peng, Alex Colburn, Qi Shan, Peter Wonka, Hung-Kuo Chu, and Derek Hoiem. Manhattan room layout reconstruction from a single 360 image: A comparative study of state-of-the-art methods. *arXiv preprint arXiv:1910.04099*, 2019. 3

[43] Zi-Xin Zou, Shi-Sheng Huang, Yan-Pei Cao, Tai-Jiang Mu, Ying Shan, and Hongbo Fu. Mononeuralfusion: Online monocular neural 3d reconstruction with geometric priors. *arXiv preprint arXiv:2209.15153*, 2022. 2